

Characterizations of contact and sheet resistances of vertically aligned carbon nanotube forests with intrinsic bottom contacts

This article has been downloaded from IOPscience. Please scroll down to see the full text article.

2011 Nanotechnology 22 365704

(<http://iopscience.iop.org/0957-4484/22/36/365704>)

View [the table of contents for this issue](#), or go to the [journal homepage](#) for more

Download details:

IP Address: 169.229.32.137

The article was downloaded on 12/08/2011 at 04:51

Please note that [terms and conditions apply](#).

Characterizations of contact and sheet resistances of vertically aligned carbon nanotube forests with intrinsic bottom contacts

Yingqi Jiang¹, Pengbo Wang^{1,2} and Liwei Lin¹

¹ Mechanical Engineering Department, University of California at Berkeley, USA

² Robotics and Microsystems Center, Soochow University, Suzhou, People's Republic of China

E-mail: jiangyq99@gmail.com and lwlin@me.berkeley.edu

Received 19 May 2011, in final form 20 July 2011

Published 11 August 2011

Online at stacks.iop.org/Nano/22/365704

Abstract

Comprehensive studies on the sheet and contact resistances of vertically aligned carbon nanotube (CNT) forests with as-grown bottom contacts to the metal layer have been conducted. Using microfabrication and four distinct methods: (1) the transfer length method (TLM), (2) the contact chain method, (3) the Kelvin method, and (4) the four point probe method, we have designed multiple testing devices to characterize the resistances of CNT-forest-based devices. Experimental results show that devices based on stripe-shaped CNT forests 100 μm in height and 100 μm in width have a sheet resistance of approximately 100 Ω/\square . The corresponding specific contact resistance to the molybdenum layer is roughly $5 \times 10^4 \Omega \mu\text{m}^2$. Consistency of the results from the four different methods validates the study. After two months of storage of the CNT forest samples in open air, less than 0.9% deviations in the resistance values were observed. We further demonstrated one application of CNT forests as an NH_3 gas sensor and measured 0.5 ppm of sensing resolution with a detection response time of 1 min.

(Some figures in this article are in colour only in the electronic version)

1. Introduction

Nanomaterials based on carbon nanotubes (CNTs) have been widely studied for various applications due to their unique characteristics including small diameters, high electrical conductivity, high surface area to volume ratio, and outstanding mechanical and thermal properties [1, 2]. Vertically aligned CNT forests could be advantageous over individual CNTs in terms of reliability, manufacturability, and structural architecture, which are all important practical issues for commercialization. For reliability considerations, bulk CNT forests can tolerate defects and failures of small numbers of CNTs within the matrix while such issues would result in system failure for devices based on individual CNTs. In terms of manufacturability, CNT forests can be easily produced in large quantities by methods such as chemical vapor deposition (CVD) at low cost [3]. In terms of structural

architecture, aligned CNT forests could be ideal materials for applications including electrodes for energy storage systems (e.g. supercapacitors [4] and batteries [5]), sensing elements for sensors [6], and interconnects in microelectronics [7] due to their intrinsic merits of orderly arrangement, natural contacts to the growth substrate, and high surface area to volume ratio.

Prior electrical characterizations of CNTs have primarily focused on individual CNTs [8–11]. For example, Frank *et al* discovered that 4 μm -long multiwalled carbon nanotubes (MWNTs) could tolerate high electrical current densities of larger than 10^7 A cm^{-2} [8] and Wei *et al* reported an even higher current carrying capacity ($J > 10^9 \text{ A cm}^{-2}$) without detectable resistance changes [9]. Javey *et al* found that contacts made of palladium (Pd) with semiconducting single-walled nanotubes (SWNTs) greatly reduced the Schottky barriers, making the 'ON' states similar to ballistic metallic tubes [10]. Recently, characterization studies have also been

done based on disoriented CNT networks. For example, Hu *et al* made a transparent SWNT network by vacuum filtration and reported a sheet resistance of $1000 \Omega/\square$ and light transmittance of 70% under visible wavelength [12]. Several research groups have also examined the properties of aligned CNT forests. Yang *et al* studied the electrical properties of CNT forests using a simple, two-terminal I - V method with gold foil in contact with the top of the CNT forests and found that the effective electrical conductances of CNT forests in the vertical and lateral directions were in the ranges of 10^4 S m^{-1} and 10^2 S m^{-1} , respectively [13]. Lin *et al* used a four point probe method by depositing titanium contact pads on the top of the CNT forest to measure their vertical and lateral electrical conductances [14]. Recently Chiodarelli *et al* used vertically aligned CNT pillars as CMOS vias and formed the contacts by evaporating Ti/Au as top electrodes and using TiN substrate as the bottom electrode [15]. These studies provide important information on the electrical characteristics of CNT forests; however, the contacts in these studies were primarily formed by depositing or establishing contacts on the top surface of CNT forests. Until now, the intrinsic contact resistance between CNT forests and the bottom substrate has not been investigated.

In fact, CNT-forest-based devices operate quite differently from devices consisting of individual CNTs and disoriented CNT networks. First, electrical current in the CNT forests flows in the horizontal direction which is perpendicular to the longitudinal direction of the individual CNTs that most other studies have reported [8–12]. As a result, the total resistance of CNT forests is strongly affected by structure properties, such as side contacts between inter-tangled CNTs. Second, the contact between CNT forests and the external world can influence the overall electrical properties. In the case of individual CNTs and disoriented CNT networks, the electrical contacts are primarily deposited after the CNT growth to form good Ohmic contacts. Electrical contacts were made similarly in previous studies for CNT forests [13–15] by adding extra metal foils or metal depositions. These top contacts are not ideal for CNT forests, because they increase the process complexity and potentially degrade the contact integrity due to mechanical fragility of the porous matrix. Furthermore, these top contacts can block external species from accessing the internal parts of the CNT forest, thereby decreasing their transport efficiency. In the majority of previous studies, CNTs have been grown predominantly on non-conducting substrates [16] such that formation of the top contacts is necessary for electrical characterizations. In this work, we used a unique combination of Mo/Al/Fe deposited on a silicon wafer to enable direct growth of CNT forests with the bottom molybdenum as the conductive layer [17]. This architecture allowed us to examine the intrinsic contact and sheet resistances for as-grown CNT forests without additional processes.

One technical challenge of the study was to separate the contact resistance from measurements that often contain unwanted resistance components. Inspired by the traditional semiconductor industry [18], we used (1) the transfer length method (TLM), (2) the contact chain method, (3) the Kelvin method, and (4) the four point probe method to measure the contact resistance. Because these methodologies have certain

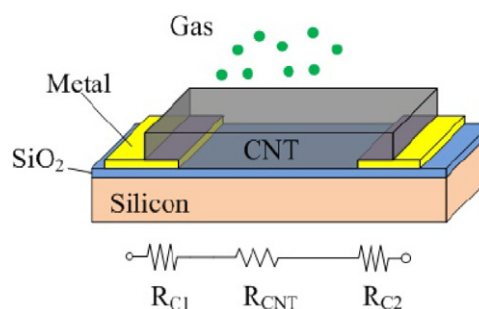


Figure 1. Schematic diagram of a testing structure used to characterize the electrical properties of the CNT forest and the demonstrative gas sensing application. The lateral sheet resistance of the CNT forest, R_{CNT} , and two CNT–metal contact resistances, R_{C1} and R_{C2} , are key components of the overall resistance of the device. When exposed to gas, the resistance of the CNT forest changes with respect to different species/concentrations of gases.

limits due to various built-in approximations, all the four schemes have been implemented and compared in this work. These as-grown CNT forests are readily available for diverse applications. We choose a resistor-based NH_3 gas sensor to demonstrate the application.

2. Design

Figure 1 illustrates the basic design configuration of this work. A silicon wafer is used as the supporting substrate and a layer of thermal oxide is grown first as the insulation layer. The metal layer, molybdenum (Mo), is used to define the contact pad areas as well as metallic interconnects. The total resistance of the device includes three components: the lateral sheet resistance of the CNT forest, R_{CNT} , and two CNT–metal contact resistances, R_{C1} and R_{C2} . For simplicity, the CNT–metal contact interface and the CNT forest on that area are treated as a whole, hereby referred to as the contact resistance in this work. The resistances of the Mo contact pads and aluminum bonding wires are small as compared to the CNT resistance and are neglected. The bottom of figure 1 shows a simplified equivalent electrical circuit model including key elements for the overall resistance. When exposed to gas, the resistance of the CNT forest changes with respect to different species/concentrations of gases such that this structure could be readily used as a gas sensor.

Figures 2(a)–(d) show the layouts of the four methods used in this work to characterize the contact and sheet resistances of CNT forests. In all designs, the CNT forests (blue color in figure 2) are $100 \mu\text{m}$ in width with variable lengths; each CNT-to-Mo contact area is $100 \times 100 \mu\text{m}^2$ in size, and the wire bonding pads are $300 \times 300 \mu\text{m}^2$.

In figure 2(a), the TLM design includes a series of CNT forest structures (devices) with identical contact pads but gradually increasing CNT resistor lengths. Therefore, the resistance of each device can be described as

$$R_{\text{M}} = x R_{\text{CNT},\square} + 2R_{\text{C}} \quad (1)$$

where R_{M} is the measured resistance, x is the number of squares of the CNT forest stripe between the two contact

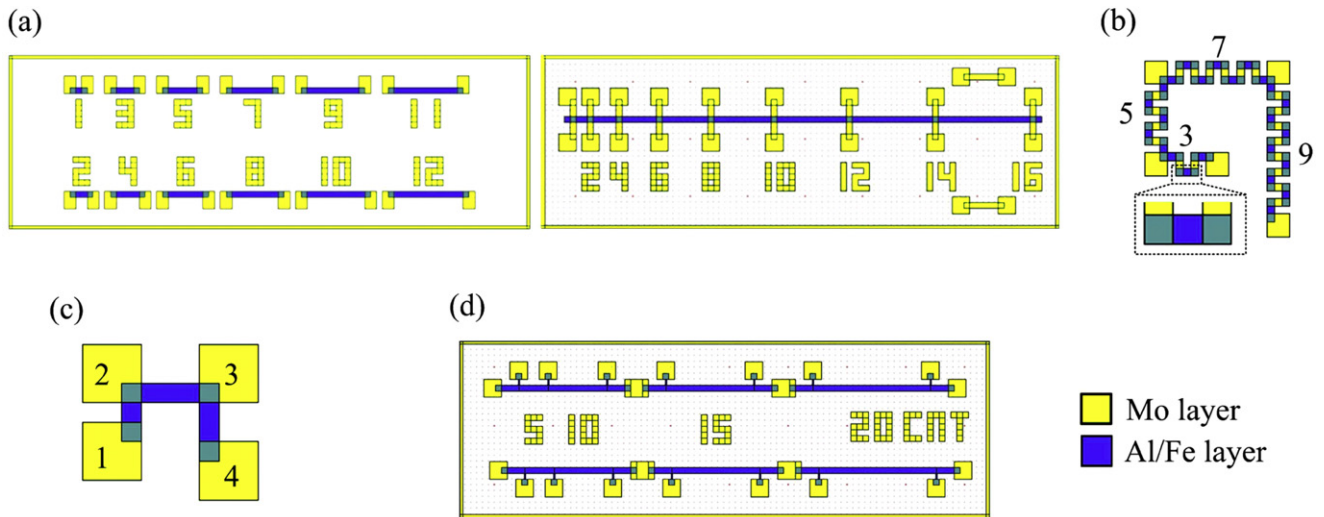


Figure 2. Device layouts of the four testing methods to characterize the sheet and contact resistances of CNT forests: (a) transfer length method (TLM), (b) contact chain method, (c) Kelvin method, and (d) four point probe method. There are two design variations for the TLM method: the one on the left is the discrete case and the one on the right is the single-line case where adjacent devices share the contact pads.

pads. One basic assumption is that the two contacts have the same contact resistance because the design configurations are symmetric and the process conditions are the same. There are two unknowns in equation (1): the sheet resistance, $R_{\text{CNT},\square}$, and the contact resistance, R_C . Mathematically, two independent equations (designs) would be enough to determine the two unknowns. However, data from only two samples often lead to large experimental errors, especially if one of the unknowns has a much smaller value than the other. Therefore, a series of CNT samples with different numbers of CNT squares ranging from 1 to 16 squares has been designed to average out the possible errors. The abundant data allow us to establish a curve between the number of squares, x , and total resistances, R_M . A linear relationship is expected where the slope of the line is the sheet resistance, $R_{\text{CNT},\square}$, and the offset of the y -axis is twice that of the contact resistance, R_C . Furthermore, two different layout designs including the discrete case and the single-line case have been implemented in the experiments. The discrete case represents the classic TLM method using separate devices, while the single-line case uses a single long CNT stripe such that the adjacent devices can share common contact pads. The latter design reduces the number of contact pads by half and conserves the device area. Note that the measurements in the single-line design were carried out only between adjacent pads (i.e., there was no additional pad between the measurement pads), thereby reducing analytical complexity.

The contact chain method in figure 2(b) resembles the TLM method with several differences: (1) the length of the CNT stripe between the contact pads is the same as one square of the CNT forest, and (2) the bonding pads are made only at the two ends of the whole CNT stripe. Therefore, each 'chain' is measured only once. For example, there are four chains in figure 2(b) with 3, 5, 7 and 9 repeating units with adjacent chains sharing the bonding pads. In each chain, the

measurement can be quantified as

$$R_M = x(R_{\text{CNT},\square} + 2R_C) \quad (2)$$

where $(R_{\text{CNT},\square} + 2R_C)$ is the resistance of a repeating unit, as shown in the enlarged portion of figure 2(b). Similarly to the TLM method, the resistance contributions made by the metal (Mo) square between repeating units are ignored. Compared to the TLM method, this design increases the relative weight of the contact resistance in the final measurements, because there are multiple contacts ($2x$) within a chain device, compared to only two contact areas in a TLM device. Using a similar plotting method to that described for the TLM method, a linear relationship between R_M and $(R_{\text{CNT},\square} + 2R_C)$ can be determined. The slope is the resistance of one repeating unit. By combining results from the contact chain method with the four point probe method to be discussed later that independently measures the sheet resistances, one can calculate the contact resistance, R_C . Another advantage of the chain design is the convenience of assessment for the yield and repeatability across large quantities of contacts by a single test.

The third design is the Kelvin structure which is a simple test structure to characterize contact resistance as illustrated in figure 2(c). A constant current (I_0) flows from pad#1 to pad#2 and a voltmeter is used to measure the voltage difference between pad#3 and pad#2. Assuming the voltmeter has an infinite internal resistance such that there is no current (voltage drop) from the CNT portion on pad#2 to pad#3, the voltage drop between pad#3 and pad#2 is, therefore, the same as the voltage drop through the contact interface between the CNT and pad#2. Thus, one single measurement reveals the contact resistance (R_C) as

$$R_C = \frac{V}{I_0}. \quad (3)$$

Similar measurements can be repeated among pad#2, pad#3, and pad#4 as well in figure 2(c). The length of the CNT portion between the contact pads is theoretically

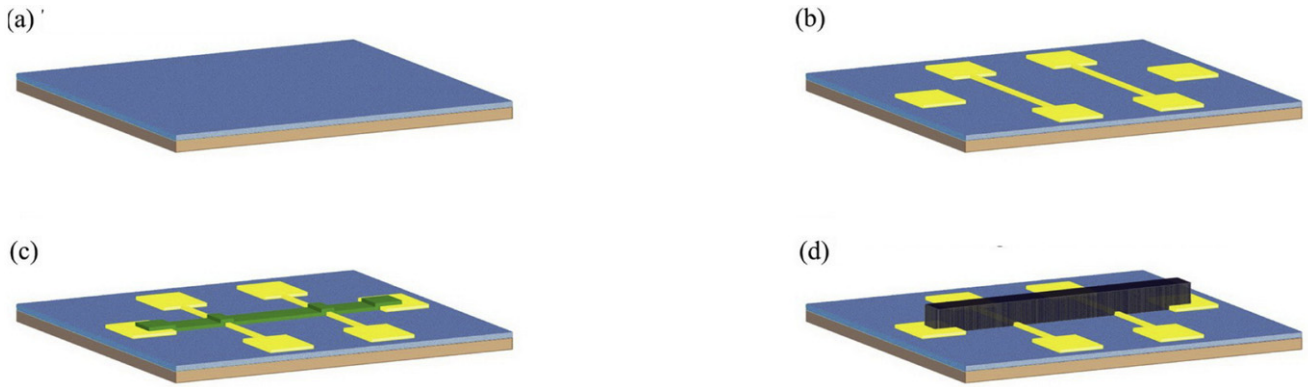


Figure 3. Fabrication process for the CNT-forest-based device. A four point probe layout is used for illustration purposes. The main process steps are (a) oxidation of silicon wafer, (b) deposition of patterned contact metal (Mo) for bonding pads and interconnections, (c) deposition of patterned CNT catalyst (Al/Fe), and (d) thermal CVD growth of CNT forest.

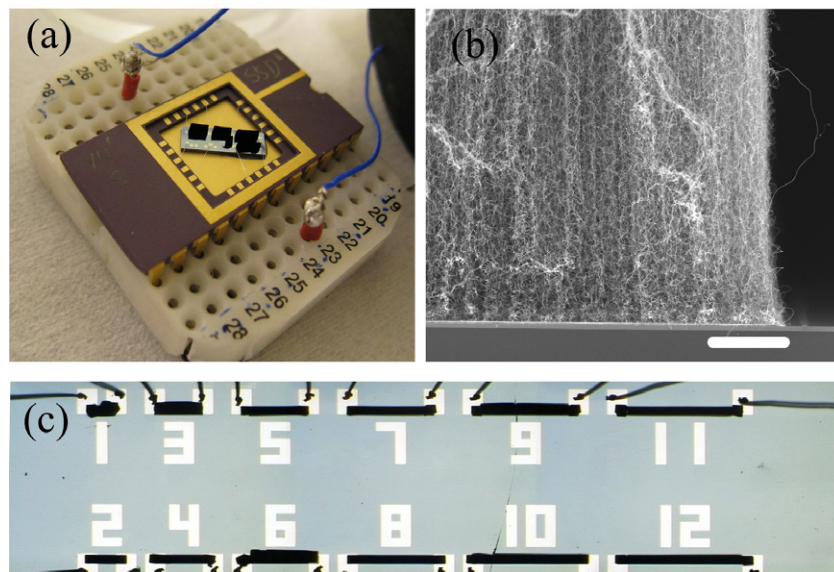


Figure 4. Fabricated samples. (a) A ready-to-test sample mounted onto a bread board. For visualization purposes the CNT samples are grown much longer than $100\ \mu\text{m}$ in height in this example. (b) The cross-sectional view at the bottom corner of a patterned CNT forest structure. The bar is $6\ \mu\text{m}$. (c) Optical picture of TLM samples (discrete case) with varying numbers of CNT squares. The width of the CNT stripes is $100\ \mu\text{m}$. The numbers on the substrate correspond to the total numbers of squares of the CNT forest devices.

irrelevant to the final results. The simplicity in terms of structure and measurement makes this method very attractive. However, unlike the previous two designs where the contact resistance can be reliably extracted from a plotting method using multiple data sources, the Kelvin method only generates one independent result, leading to a relatively larger volatility. Despite the limitation, the Kelvin structure still provides an effective and simple alternative way to characterize contact resistance.

Figure 2(d) shows the four point probe design, which is well known to eliminate the effect of contact resistances, and the sheet resistance can be calculated by using the equation

$$R_M = x R_{\text{CNT},\square} = \frac{V}{I_0} \quad (4)$$

where x is the number of CNT squares between the two middle probes, V is the measured voltage drop between the

two middle probes and I_0 is the applied constant current. Due to the advantages of microfabrication processes, the middle probes in our design are only $20\ \mu\text{m}$ in width, which enables higher accuracy for measuring the voltage and counting the squares. As described previously, when combined with the contact chain method, contact resistances can be derived.

3. Fabrication

Figure 3 shows the fabrication process. First, a silicon wafer is thermally oxidized to provide an electrically insulating substrate. Afterward, the first lithography step is used to define the bonding pads as well as other electrically conductive areas. Using the lift-off process, $50\ \text{nm}$ thick molybdenum (Mo) is deposited by evaporation and patterned. The CNT growth areas are defined by a second aligned lithography. Using a second

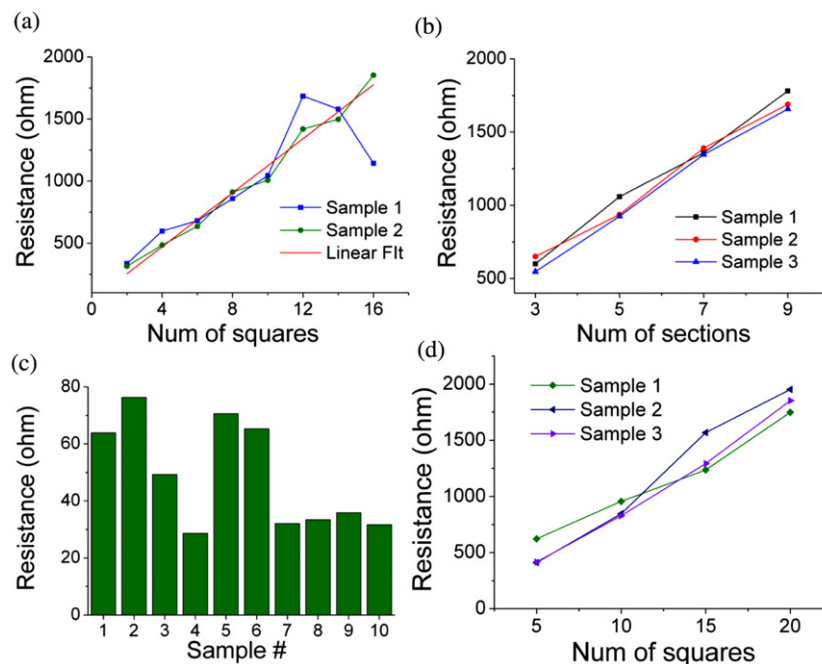


Figure 5. Experimental results from the four testing methods. (a) TLM method using different lengths of CNT forest samples and two contacts. (b) Contact chain method using repeating units comprised of two metal contacts and one square of CNT forest. (c) Kelvin method. A known current flows through CNT–metal contacts while the voltage drop through the interface is measured from nearby pads. (d) Four point probe method.

Table 1. Summary of the calculated results for the four designs. The contact area is $100 \times 100 \mu\text{m}^2$ in all samples. The CNT forest test sample is $100 \mu\text{m}$ in height and $100 \mu\text{m}$ in width.

Method	TLM (discrete)	TLM (single line)	Contact chain	Kelvin method	Four probe method
Sheet resistance (Ω/\square)	$99.3(\pm 3.3)$	$108(\pm 6)$	N/A	N/A	95.5 ± 4.7
Contact resistance (Ω)	$62(\pm 12)$	$18(\pm 30)$	$<43.5(\pm 4)$	~ 49	N/A

lift-off process, aluminum (Al) and iron (Fe) are evaporated with thicknesses of 10 nm and 5 nm, as supporting and catalyst layers, respectively. Finally, thermal CVD growth of the CNTs is achieved in a 2 in quartz tube with pre-mixed ethylene (C_2H_4) and hydrogen (H_2) gas flow at a ratio of 611:90 (unit: sccm). The growth temperature is set at 720°C and the growth time is controlled to be 10 min. These parameters result in CNT forests of approximately $100 \mu\text{m}$ in height. The device is finally mounted to a ceramic package and connected using wire bonding. Figure 4(a) shows a ready-to-test sample that was mounted onto a bread board and figure 4(b) is the cross-sectional view at the bottom corner of a patterned CNT forest stripe. Vertically aligned CNTs can be clearly identified. The optical picture in figure 4(c) shows TLM samples of different lengths and the numbers in the photo correspond to the numbers of squares of the different samples. The major problem we experienced in the process was that some CNT stripes incidentally broke at the edges between the regions with and without the Mo bottom layer possibly due to uneven growth caused by the bottom Mo layer. Fortunately, most fabrication runs do not have this problem and we believe this issue can be eventually eliminated by optimization of the fabrication process.

4. Results and discussion

Measurement results are presented in figures 5(a)–(d). Figure 5(a) shows results from the TLM design (single-line case) with a linear relationship between R_x and the total number of squares. The slope of the line is the sheet resistance of the CNT forest and the y-axis offset represents the value of $2R_C$. Two sets of up to 16 square resistor samples have been measured, and minor fluctuations along the best linear fit line have been observed. The unusual large deviations in sample #1 for tests on the ‘12’ and ‘16 square’ samples are due to the formation of cracks of the CNT forest at the intersection between the oxidized substrate and the metal pads as discussed previously. Figure 5(b) shows results from the contact chain method. A linear relationship between R_x and the number of repeating units was clearly observed as expected. Because these contacts were connected in series, any single bad contact would have resulted in accumulative large measurement errors. However, since only small fluctuations were observed, this implies good repeatability of the contacts between the CNT forests and the metal. Measurement results from the Kelvin method are shown in figure 5(c) and these data were collected from individual samples which results in relatively large fluctuations. The measured contact resistances

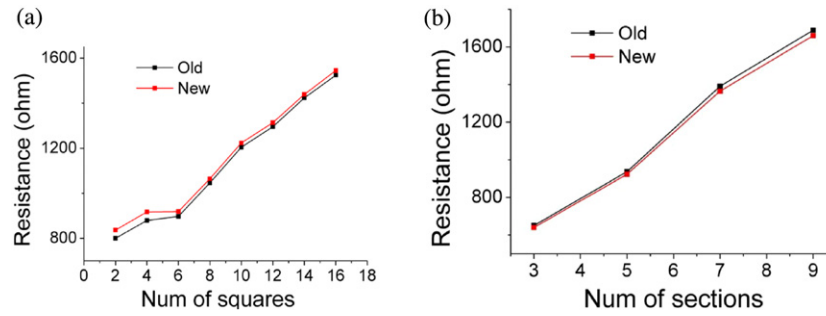


Figure 6. Resistance measurement results from initial data and after storage in open-air conditions for two months. (a) Single-line TLM design, and (b) contact chain design.

are in the range of 30–80 Ω for ten individual samples and the average contact resistance is calculated as 49 Ω . Finally, results from the four point probe design are plotted in figure 5(d) with the expected linear behavior and the sheet resistance is calculated as 95.5 Ω/\square .

Table 1 summarizes the calculated results and standard deviations based on the data shown in figure 5 from the four different methods. In general, the sheet resistance of the 100 μm (H) \times 100 μm (W) CNT forest is approximately 100 Ω/\square from both the TLM and four point probe methods. The contact resistance of the CNT forest and Mo is roughly 50 Ω for a contact area of 100 \times 100 μm^2 from the TLM, contact chain, and Kelvin methods. From the results presented in [15] which used a CNT forest with evaporated Ti/Au as the top electrode and a TiN substrate, a contact resistance of $4.72 \times 10^4 \Omega \mu\text{m}^2$ can be calculated, which is about one order of magnitude lower than this work at $5 \times 10^5 \Omega \mu\text{m}^2$. The major reason is that CNT contacts with different metal layers can make big differences. Other parameters in the growth process (temperature, gas concentration, ...) are also factors which can result in different contact resistances. The single-line case of the TLM method has a standard deviation of 30 Ω for the contact resistance, larger than the measured contact resistance value, 18 Ω . This comes from the fact that the contact resistance is relatively small compared to the CNT forest's bulky resistance such that the possible measurement errors for the CNT sheet resistance dominate the calculations. Fortunately, this confusion can be cleared by considering results from other methods as presented in this work. Therefore, measurements from multiple independent methods, instead of a single method, provide more reliable characterization results.

Furthermore, the resistivity of the CNT forest can be calculated from the sheet resistance equation

$$R_{\text{CNT},\square} = \frac{\rho_{\text{CNT}}}{H_{\text{CNT}}} \quad (5)$$

where ρ_{CNT} represents the resistivity of the CNT forest and H_{CNT} is the height of the forest. One can obtain a CNT forest resistivity of about 1 $\Omega \text{ cm}$ (alternatively, a conductivity of 1 $\Omega^{-1} \text{ cm}^{-1}$), which is consistent with some of the prior reports [13, 14]. The sheet resistance of the same type of CNT forest with different heights can be calculated accordingly.

For practical applications, it is important to further investigate the long-term stability of the CNT samples. For this purpose, resistance characterizations were conducted again after the initial measurements and the storage of the samples in an unsealed box for two months. Figures 6(a) and (b) show representative experimental results for the samples using the single-line TLM and contact chain designs, respectively. In general, resistance changes after two months were minimal, with slight increase and decrease of resistance in figures 6(a) and (b), respectively. The relatively larger variations in figure 6(a) for the '2' and '4 square' samples were likely caused by pre-existing cracks in the CNT forests. Without counting these two values, the maximum resistance changes in both samples are only 0.9%. Considering the small variations in these experiments, as well as the possible influences of gas and moisture in the air, the CNT forest structures were able to maintain their resistance values remarkably well.

5. Gas sensing demonstration

Many research groups have used individual CNTs and disoriented CNT networks as sensing materials [19–24]. Kong *et al* made chemical sensors based on individual SWNTs and observed the conductance of the SWNT sample to significantly decrease with response times of 1–2 min after exposure to 1% NH_3 [19], but the sensor required hours to recover most of its original resistance under the ambient condition. Electrothermal effects of a single MWNT have also been demonstrated for pressure and gas sensing applications [20]. Recently researchers have used disoriented CNT networks as gas sensors with good sensitivity and stability [21, 22] and both the sensitivity and the selectivity of CNT-based sensors have been further enhanced by functionalization of the CNTs [23, 24]. Compared to gas sensors based on individual CNTs or CNT networks, vertically aligned CNT forests could be beneficial in terms of yield and reproducibility. For example, Penza *et al* have reported a miniaturized gas sensor to monitor landfill gases using metal-modified, aligned CNT forests [25]. The CNT forest samples presented in this work can be readily employed as chemiresistor gas sensors. In contrast to the aforementioned previous works where electrodes were deposited on top of the CNT forest [25], this work can use the metal bottom electrodes without extra deposition.

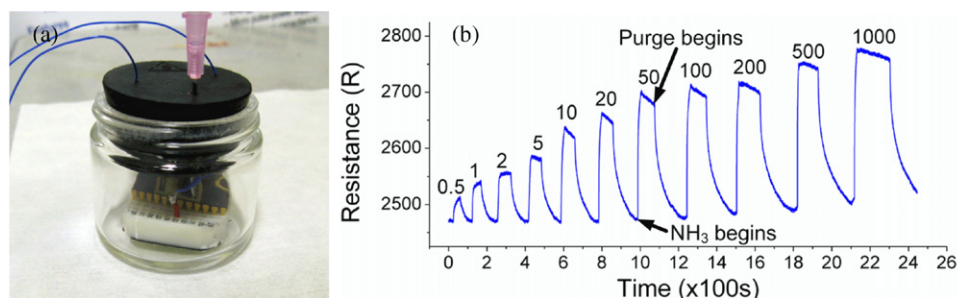


Figure 7. Gas sensing using the CNT forest. (a) Homemade test setup, (b) sensing results with different NH₃ gas concentrations. The arrows give the example when the NH₃ and air were pushed in. The unit for NH₃ in the figure is ppm.

NH₃ was chosen for the gas sensing demonstration and possible comparison with results from other similar works. Figure 7(a) shows the experimental setup where a prototype device was placed inside a sealed bottle. The chamber was filled with NH₃ of different concentrations and vented with air alternately. A constant voltage was applied on the CNT samples and the current was monitored simultaneously to obtain the CNT resistance values. When exposed to NH₃, a rapid increase of CNT resistance was observed. Afterward, air was used to purge the chamber and the resistance of the CNT sample returned to the initial value, as shown in figure 7(b). The experimental results suggest that the absorption of NH₃ gas molecules on CNTs hinders the electron transfer process within the tubes such that the resistance is increased. Conversely, the desorption process of NH₃ molecules during the air venting process leads to a recovery of the initial resistance. Furthermore, the detection process is quick and reversible. Preliminary results show that the sensor response time is about 1–2 min with a broad sensing range for NH₃ concentration from 0.5 to 1000 ppm and a minimum demonstrated resolution of 0.5 ppm.

Based on a single semiconductor SWNT (single-walled CNT) device, the paper [19] has reported about 100 times conductance reduction when it was exposed to 1% NH₃ and only 1.5 times reduction for an SWNT mat. The CNT forest gas sensor here has about 1.12 times resistance increment at 1000 ppm (0.1%) NH₃. Several differences between these devices contribute the variations. First, a semiconducting SWNT could be much more sensitive to exterior influences than either metallic SWNTs or MWNTs as much reduced sensitivity was reported in [19] by using a single metallic SWNT. Second, in contrast to the longitudinal direction of electron movement along the SWNT, electrons move laterally on the vertically aligned CNT forest or perpendicular to the longitudinal direction of the CNTs. Nevertheless, the sensitivity of the prototype device is of the same order of magnitude as the SWNT mat. Furthermore, the prototype device has a time response of 1–2 mins which is also comparable with the previous report in [19] of 2 min for a single semiconducting SWNT, yet better than 10 min for an SWNT mat. One possible reason is that the MWNT forest has large intervals between individual CNTs for fast transport of gas molecules.

6. Conclusions

We have applied four distinct methods to characterize the contact and sheet resistances of vertically aligned CNT forests with bottom metal contacts with relatively consistent results. Experimental results show that, for CNT stripes $100 \times 100 \mu\text{m}^2$ in cross-sectional area of height and width, the sheet resistance is approximately $100 \Omega/\square$ while the contact resistance is roughly 50Ω for a CNT–Mo contact with an area of $100 \times 100 \mu\text{m}^2$. The long-term stability of CNT-forest-based devices has been investigated by conducting resistance measurements on the same as-fabricated devices after two months of storage in air. The experimental results suggest minimal changes in CNT resistance. Furthermore, the application of CNT forest samples as NH₃ gas sensors has been demonstrated with a resolution of 0.5 ppm and a response time of 1 min. Our results suggest that CNT-forest-based devices could yield promising applications in a variety of fields. The characterization methodologies and measured material properties presented here provide support for future efforts in utilizing CNT forests for practical applications.

Acknowledgment

This project is supported in part by the DARPA N/MEMS Fundamentals Program and Siemens Inc.

References

- [1] Baughman R H, Zakhidov A A and de Heer W A 2002 Carbon nanotubes—the route toward applications *Science* **297** 787–92
- [2] Jorio A, Dresselhaus G and Dresselhaus M S 2008 *Carbon Nanotubes: Synthesis, Structure, Properties and Applications* (Berlin: Springer)
- [3] Cassell A M, Raymakers J A, Kong J and Dai H 1999 Large scale CVD synthesis of single-walled carbon nanotubes *J. Phys. Chem. B* **103** 6484–92
- [4] Pushparaj V L, Shaijumon M M, Kumar A, Murugesan S, Ci L, Vajtai R, Linhardt R J, Nalamasu O and Ajayan P M 2007 Flexible energy storage devices based on nanocomposite paper *Proc. Natl Acad. Sci.* **104** 13574–7
- [5] Welna D T, Qu L, Taylor B E, Dai L and Durstock M F 2011 Vertically aligned carbon nanotube electrodes for lithium-ion batteries *J. Power Sources* **196** 1455–60
- [6] Jiang Y, Wang P and Lin L 2011 Contact and sheet resistances of carbon nanotube forest in gas sensing applications *IEEE MEMS Conf. 2011 (Cancun, Jan. 2011)* pp 396–9

- [7] Banerjee K, Li H and Srivastava N 2008 Current status and future perspectives of carbon nanotube interconnects *8th IEEE Conf. on Nanotechnology (Arlington, TX, Aug. 2008)* pp 432–6
- [8] Frank S, Poncharal P, Wang Z L and de Heer W A 1998 Carbon nanotube quantum resistors *Science* **280** 1744–6
- [9] Wei B Q, Vajtai R and Ajayan P M 2001 Reliability and current carrying capacity of carbon nanotubes *Appl. Phys. Lett.* **79** 1172–4
- [10] Javey A, Guo J, Wang Q, Lundstrom M and Dai H 2003 Ballistic carbon nanotube field-effect transistors *Nature* **424** 654–7
- [11] Kawano T, Christensen D, Chen S, Cho C Y and Lin L 2006 Formation and characterization of silicon/carbon nanotube/silicon heterojunctions by local synthesis and assembly *Appl. Phys. Lett.* **89** 163510
- [12] Hu L, Hecht D S and Gruner G 2004 Percolation in transparent and conducting carbon nanotube networks *Nano Lett.* **4** 2513–7
- [13] Yang D J, Wang S G, Zhang Q, Sellin P J and Chena G 2004 Thermal and electrical transport in multi-walled carbon nanotubes *Phys. Lett. A* **329** 207–13
- [14] Lin C T, Lee C Y, Chin T S, Xiang R, Ishikawa K, Shiomi J and Maruyama S 2011 Anisotropic electrical conduction of vertically-aligned single-walled carbon nanotube films *Carbon* **49** 1446–52
- [15] Chiodarelli N *et al* 2011 Measuring the electrical resistivity and contact resistance of vertical carbon nanotube bundles for application as interconnects *Nanotechnology* **22** 085302
- [16] Talapatra S, Kar S, Pal S K, Vajtai R, Ci L, Victor P, Shajumon M M, Kaur S, Nalamasu O and Ajayan P M 2006 Direct growth of aligned carbon nanotubes on bulk metals *Nature Nanotechnol.* **1** 112–6
- [17] Jiang Y, Zhou Q and Lin L 2009 Planar MEMS supercapacitor using carbon nanotube forests *IEEE MEMS 2009 Conf. (Sorrento, Jan. 2009)* pp 587–90
- [18] Schroder D K 2006 *Semiconductor Material and Device Characterization* 3rd edn (Hoboken, NJ: Wiley)
- [19] Kong J, Franklin N R, Zhou C, Chapline M G, Peng S, Cho K and Dai H 2000 Nanotube molecular wires as chemical sensors *Science* **287** 622–5
- [20] Kawano T, Chiamori H C, Suter M, Zhou Q, Sosnowchik B D and Lin L 2007 An electrothermal carbon nanotube gas sensor *Nano Lett.* **7** 73686–90
- [21] Li J, Lu Y, Ye Q, Cinke M, Han J and Meyyappan M 2003 Carbon nanotube sensors for gas and organic vapor detection *Nano Lett.* **3** 929–33
- [22] Snow E S, Perkins F K, Houser E J, Badescu S C and Reinecke T L 2005 Chemical detection with a single-walled carbon nanotube capacitor *Science* **307** 1942–5
- [23] Star A, Joshi V, Skarupo S, Thomas D and Gabriel Gas J P 2006 Sensor array based on metal-decorated carbon nanotubes *J. Phys. Chem. B* **110** 21014–20
- [24] Zhang T, Mubeen S, Bekyarova E, Yoo B Y, Haddon R C, Myung N V and Deshusses M A 2007 Poly(m-aminobenzene sulfonic acid) functionalized single-walled carbon nanotubes based gas sensor *Nanotechnology* **18** 165504
- [25] Penza M, Rossi R, Alvisi M and Serra E 2010 Metal-modified and vertically aligned carbon nanotube sensors array for landfill gas monitoring applications *Nanotechnology* **21** 105501